PCCP

Accepted Manuscript

ROYAL SOCIETY OF CHEMISTRY

www.rsc.org/pccp

Molecular Oxygen Reduction Catalyzed by a Highly Oxidative Resistant Complex of Cobalt-Hydrazone at Liquid/Liquid Interface

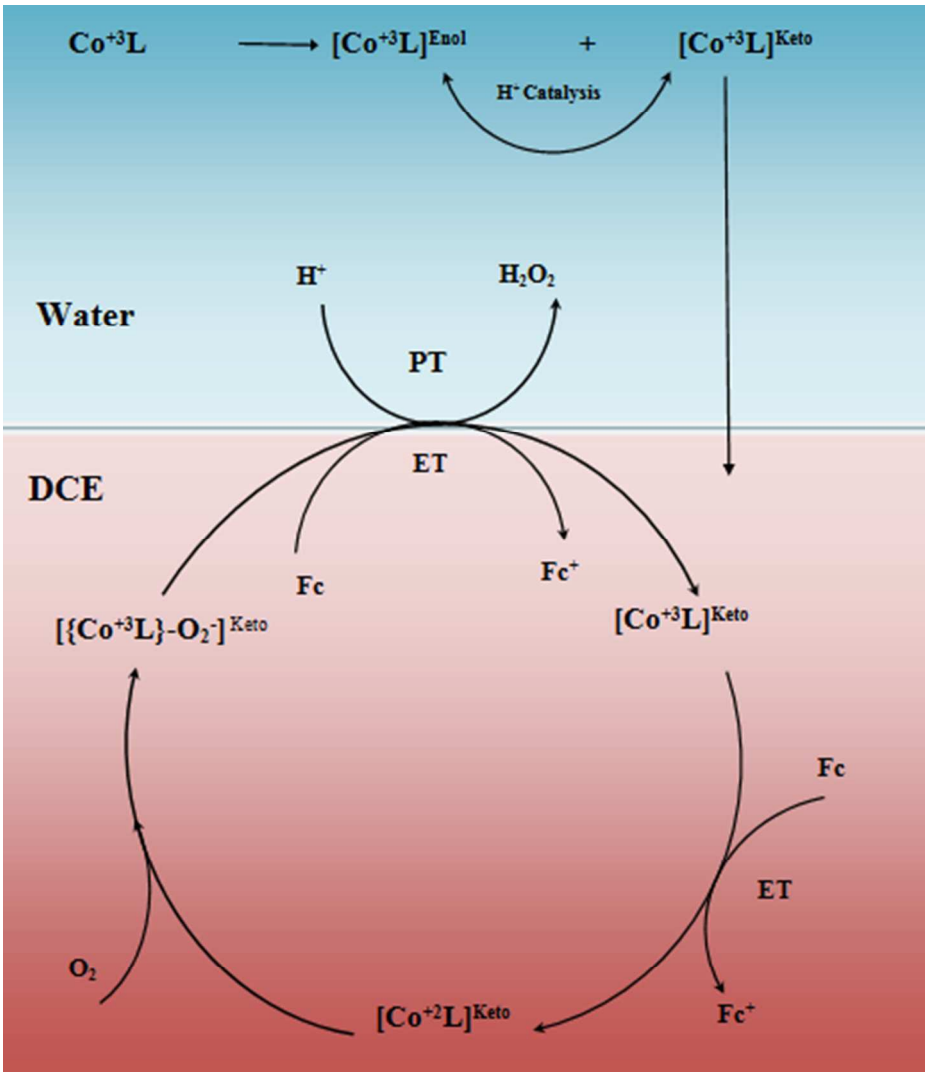

Highlights

- ✓ Syntheses, structure and spectroscopic studies of a new cobalt complex with hydrazine ligand
- ✓ First report on a highly oxidative resistant complex in the ORR electrocatalystsis
- ✓ Electrocatalysis of oxygen reduction at liquid-liquid interface

Molecular Oxygen Reduction Catalyzed by a Highly Oxidative Resistant Complex of Cobalt-Hydrazone at Liquid/Liquid Interface

Mohammad-Ali Kamyabi[a,*], Fatemeh Soleymani-Bonoti[a], Rahman Bikas[a], Hassan Hosseini-Monfared[a], Nematollah Arshadi[a], Milosz Siczek[b] and Tadeusz Lis[b]

[a] *Department of Chemistry, Faculty of Science, University of Zanjan 45371-38791, Zanjan, Iran*

[b] *Faculty of Chemistry, University of Wroclaw, Joliot-Curie 14, Wroclaw 50-383, Poland*

Abstract

A new complex of Co(III) using a oxidative stable hydrazone ligand, CoL, was synthesized and characterized by elemental analysis, spectroscopic methods and single crystal X-ray analysis where HL is bis-[(*E*)-*N*′-(phenyl(pyridin-2-yl)methylene)]carbohydrazide. X-ray analysis revealed that the complex is a mononuclear and the coordination environment around the Co(III) core is *trans*-[CoN_4Cl_2]. The catalytic activity of the complex in oxygen reduction reaction was investigated. The complex is a highly oxidative resistant cobalt-hydrazone which can efficiently catalyze the reduction of oxygen (O_2) by a weak electron donor ferrocene, (Fc), at the polarized water/1,2-dichloroethane (DCE) interface. Oxygen reduction is coupled with proton transfer from water to the organic phase to form hydrogen peroxide, which is extracted into the aqueous phase.

Keywords: Proton-Coupled O_2 Reduction; Liquid/Liquid Interfaces; Carbohydrazone; Cobalt complex; Crystal structure

[*] Corresponding author. Tel.: +98 24 33052617; fax: +98 24 5283203.*E-mail address*: makamyabi@gmail.com (M.A. Kamyabi).

1. Introduction

Molecular oxygen reduction reaction, (ORR), is an interesting subject in energy conversion systems such as fuel cells, metal-air batteries, corrosion and in life processes such as biological respiration.[1] ORR can proceed by a direct four-electron reduction to produce water or a two-electron reduction to give hydrogen peroxide.[2] Hydrogen peroxide is an important chemical due to its attractive features like anti-bacterial property, decolorizing and oxidizing agent.[3] Moreover, its outstanding application in fuel cells as a carbon-free energy carrier and a strong oxidant in direct peroxide–peroxide fuel cell are recently developed.[4]

In nature, oxygen reduction occurs at soft interfaces, namely biomembranes that provide both a physical separation of the reactants and products, and an electrochemical driving force resulting from the membrane electrical potential difference. Electrochemistry at liquid-liquid interfaces is a new type of bioinspired electrochemistry.[5]

Electrocatalysis at the liquid/liquid interface, or the so-called interface between two immiscible electrolyte solutions (ITIES), has recently attracted a great deal of research interest and has been applied to study the oxygen reduction reaction (ORR),[6] hydrogen evolution[7] and carbon dioxide reduction.[8] The liquid/liquid phase boundary offers the possibility to physically separate reactants and to control the flux of either ion (*e.g.*, proton) or electron transfer, which is particularly interesting when considering the ORR as it is a proton-coupled electron-transfer (PCET) reaction.[1] These reactions can be driven by the interfacial potential difference, called the Galvani potential difference, which can either be controlled potentiostatically using a four-electrode potentiostat or chemically by two-phase shake flask experiments.[9] Oxygen reduction at the ITIES has been extensively studied using various lipophilic electron donors, decamethylferrocene (DMFc),[10] reduced flavin mononucleotide (FMN),[11] tetrachlorohydroquinone (CQH_2)[12] and fullerene monoanion ($C60^-$).[13] Furthermore, the catalytic effect of various metalated[9,14] or free base monomeric porphyrin compounds,[15] metallic phthalocyanines[16, 17]

and various ligand[18,19] as well as electrodeposited platinum particles[10] on the oxygen reduction by ferrocene derivatives at the water/DCE interface have also been investigated.

A Schiff base is a compound with a functional group that contains a carbon-nitrogen double bond, with the nitrogen atom connected to an aryl or alkyl group but not hydrogen.[20] Hydrazones are a special group of compounds in the Schiff base family. They are characterized by the presence of the RR'C=N–NH–C(=O)R" moiety, where R, R' and R" can be H, alkyl or aryl groups. These ligands, due to their facile keto-enol tautomerization and the availability of several potential donor sites (depending on the nature of the substituent's attached to the hydrazone unit), represent good polydentate chelating agents with interesting modes of ligation for a variety of metal ions.[21,22] The chemistry of hydrazone based ligands and their transition metal complexes is a broad research field between coordination chemistry, analytical chemistry, biochemistry and catalysis.[23] These ligands create various coordination environments similar to biological systems by coordinating through oxygen and nitrogen atoms.[24] Therefore, they are target molecules for mimicking the behavior of several biological systems. Hydrazone complexes of transition metals are stable during the oxidation of hydrocarbons. Various complexes of Schiff base ligands have been used as catalysis for the electro reduction of O_2 to H_2O.[22]

The transition metal complexes of Schiff bases are important in scientific interest because of multiple applications.[25,26] Some of such complexes are able to bind reversibly molecular oxygen, being used as simplified models in the study of dioxygen fixation by its natural transporters and mimic the biological oxidation. The Schiff base complexes are also involved in the study of the artificial metallo proteins and metallo enzymes.[27]

Cobalt(III) and nickel(II) complexes of multidentate Schiff base ligands have been extensively used[28] because of these ligands can bind with one or more metals involving various coordination modes and allow the synthesis of homo- and/or hetero nuclear metal complexes with interesting stereochemistry.[29] Cobalt chelate complexes are useful in highly selective catalytic oxidation reactions

using molecular oxygen, as models for oxygenases, peroxydases or mono- and dioxygenases.[30] The cobalt Schiff base complex can catalyze the oxidation of phenols, alcohols, flavonoides, nitroalcanes, hydrazines or olefins and electro-reduction.[31]

Considering the application of cobalt complexes in catalytic O_2 reduction reactions, here we report the synthesis, characterization and catalytic behavior of a new complex of a hydrazone ligand $[Co(L)Cl_2]\cdot CH_3OH$ (HL = bis-[(E)-N'-(phenyl(pyridin-2-yl)methylene)]carbohydrazide) which is shown by CoL. The complex efficiently catalyzes the reduction of O_2 at the water/DCE interface where the aqueous phase is acidic and the organic phase contains ferrocene, (Fc), as an electron donor. Fc alone performs the reduction of oxygen very slowly. Most of the reported electrocatalyst compounds for reduction of oxygen suffer from decomposing in the medium of hydrogen peroxide which is produced during the reaction, but the hydrazone complex used in this study is stable.[23,32] Biphasic reactions show that CoL catalyzes the reduction of oxygen mainly to H_2O_2. Ion transfer voltammetry results suggest that the voltammetric current signal observed in the presence of aqueous acid, CoL, Fc and O_2 corresponds to a PCET reaction.

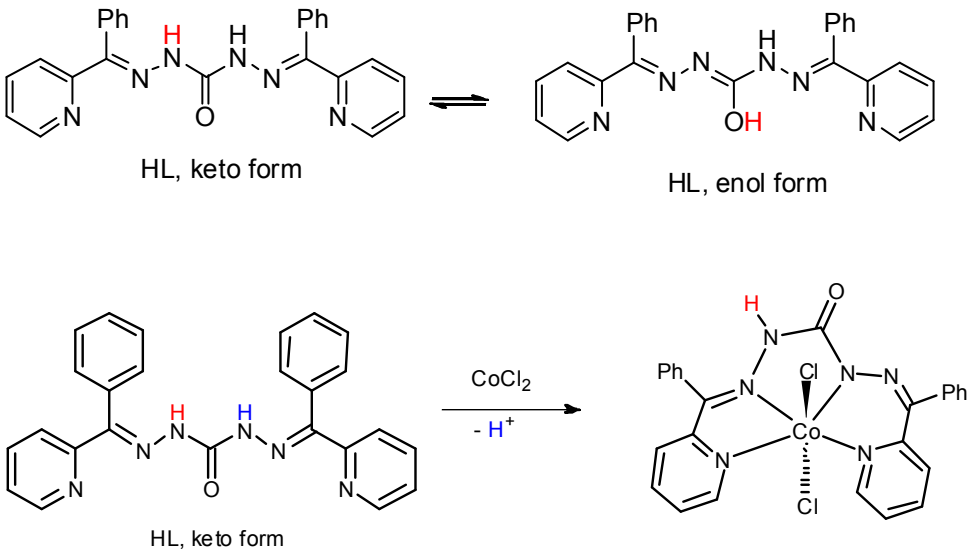

Scheme 1. The tautometric forms of HL and formation of the complex CoL

2. Experimental Section

2.1 Materials and instrumentations

Solvents of the highest commercially available grade (Merck) were used without further purification. Bis(triphenylphosphoranylidine)ammonium chloride (BACl 98%), lithium tetrakis(pentafluorophenyl)borate ethyl etherate (LiTB purum) and lithium chloride (LiCl>99%), Potassium iodide (KI, 99%) and ferrocene, (Fc, 98%), were purchased from Sigma-Aldrich. Hydrochloric acid (37%) and 1,2-dichloroethane (DCE) were purchased from Merck. Cobalt(II) chloride hexahydrate, carbohydrazide and 2-benzoylpyridine were purchased from Across and used as received.

Bis(triphenylphosphoranylidine)ammonium tetrakis(pentafluorophenyl) borate (BATB) was prepared by a metathesis of 1:1 mixture of BACl and LiTB in methanol/water (V:V = 2:1), followed by recrystallization from acetone. IR spectra were recorded as KBr disks with a Bruker FT–IR spectrophotometer. UV–Vis spectra of solutions were recorded on a HACH (DR 5000) spectrophotometer. ^{1}H and ^{13}C NMR spectra of ligand in DMSO-d_6 solution were measured on a Bruker 250and 62.50 MHz spectrometer, respectively, with chemical shifts indicated in ppm relative to tetramethylsilane. The atomic absorption analysis was carried out using Varian Spectra AA-220 equipment.

2.2. Synthesis of bis-[(E)-N'-(phenyl(pyridin-2-yl)methylene)]carbohydrazide (HL)

The reaction of carbohydrazide with 2-benzoylpyridine in methanol gave the desired Schiff base ligand (HL). Briefly, a methanol (10 mL) solution of 2-benzoylpyridine (1.10 g, 6.00 mmol) was added drop-wise to a methanol solution (10 mL) of carbohydrazide (0.27 g, 3.00 mmol) and the mixture refluxed for 6 h. The solution was then evaporated on a steam bath to a volume of 5 cm^3 and cooled to room temperature. The resulting white precipitate was separated and filtered off, washed with 5 mL of cooled

methanol and re-crystallized. Yield: 92% (1.16 g). *Anal*. Calc. for $C_{25}H_{20}N_6O$ (MW = 420.47): C, 71.41; H, 4.79; N, 19.99. Found: C, 71.44; H, 4.77; N, 20.02%. The details of the characterization of HL is given in the Supporting Information file (Section I).

2.3. Synthesis of the catalyst CoL

The reaction of HL and cobalt(II) chloride hexahydrate in methanol led to an octahedral complex of Co(III), CoL. This complex was synthesized by the reaction of carbohydrazone ligand, HL, (0.42 g, 1.0 mmol) and $CoCl_2 \cdot 6H_2O$ (0.24g, 1.0 mmol) using a thermal gradient method in a branched tube and with methanol as solvent. For this purpose, mentioned amount of materials were placed in the main arm of a branched tube. Methanol was carefully added to fill both arms, the tube was sealed and arm containing the reagents immersed in an oil bath at 60 °C, while the other arm was kept at ambient temperature. After a week, dark brown crystals of the complex were deposited in the cooler arm, which were filtered off and air dried. Yield: 86% (0.50g). *Anal.* Calc. for $C_{26}H_{23}Cl_2CoN_6O_2$ (MW = 581.33): C, 53.72; H, 3.99; N, 14.46; Co, 10.14%. Found: C, 53.78; H, 4.02; N, 14.37; Co, 10.06%. The details of the characterization of the catalyst CoL is given in the Supporting Information file (Section II).

2.4. X-ray crystallography

X-ray diffraction data for the complex was collected at 100 K by the ω-scan technique on Kuma KM4 CCD diffractometer with CCD-detector using graphite-monochromatized MoK_α radiation (λ=0.71073 Å). Data were corrected for Lorentz-polarization effects as well as for absorption. The structure was solved with SHELXS97 and refined with the full-matrix least-squares procedure on F^2 by SHELXL97[33] Scattering factors incorporated in SHELXL97 were used.

2.5. Electrochemical measurements

Electrochemical measurements at the water/DCE interface were performed in a four-electrode configuration on a commercial micropotentiostat (PGSTAT 101, Eco-Chemie). The electrochemical cell was used a three-compartment glass cells. Two platinum counter electrodes were positioned in the aqueous and DCE phases, respectively, to supply the current flow. An external potential was applied between two reference electrodes, silver/silver chloride (Ag/AgCl), which connected to the aqueous and DCE phases respectively by means of a Luggin capillary. Electrolyte compositions are illustrated in Scheme 2. The potential was converted to the Galvani potential difference ($\Delta_O^W\Phi$), based on cyclic voltammetric measurement of the reversible half-wave potential of the TMA^+ cation transfer (0.16 V).[34] All electrochemical measurements were performed at ambient temperature (23 ± 2^0C).

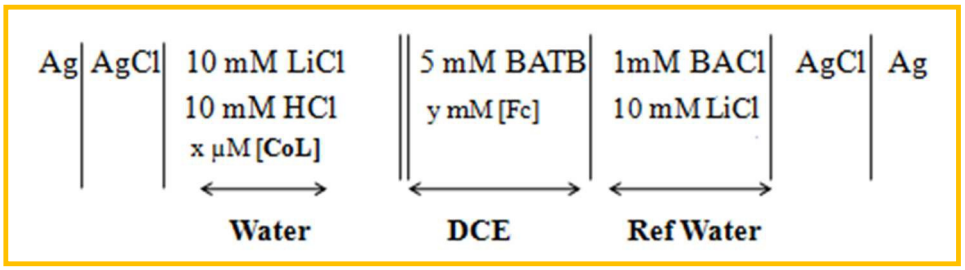

Scheme 2. Composition of the electrochemical cell

2.6. Shake flask experiments

The two-phase reactions were performed in a small flask under stirring conditions for 50 min. Firstly, the DCE solution (1 mL) containing 5 mM Fc was added to the flask, followed by the addition of 1 mL of aqueous solution containing 57 µM of CoL and 32 mM of HCl. The LiTB salt was added at a

concentration of 5 mM to the aqueous phase to produce the common ion (TB^-). After stirring for 50 min and waiting for the clear separation of two phases, the aqueous and organic solutions were isolated from each other. The aqueous solution was treated by excess amount of KI and used for UV-Vis spectra, while the organic solution was directly subjected to UV-visible spectroscopic measurements.

3. Results and Discussion

3.1. Spectroscopy and X-ray structure

3.1.1. Spectroscopy of HL and CoL

The UV-Vis spectrum of HL shows two bands at 270 and 290 nm. Based on their extinction coefficients, they can be attributed to $\pi \rightarrow \pi^*$ transitions (Fig. 1). The UV–Vis spectrum of CoL in water shows three absorbance bands at 510, 390 and 270 nm, which can be due to the charge transfer (LMCT) transitions.

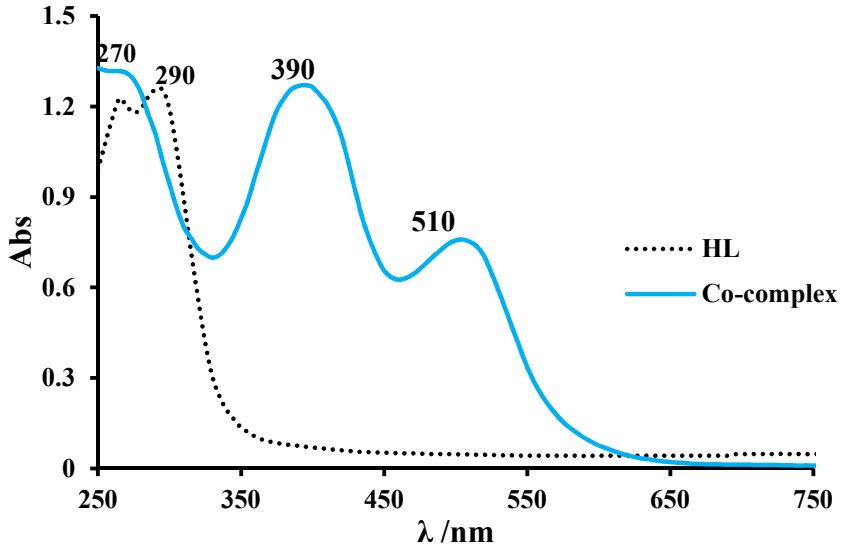

Fig 1. UV−Vis spectra of complex CoL (c = 60 μM) and HL (c = 100 μM) in aqueous solution

3.1.1. X-ray structure of CoL

Crystallographic data are listed in Supporting Information file Table S_1 Section (II). All non-hydrogen atoms were refined anisotropically, all hydrogen atoms were placed in calculated positions and were refined as 'riding' on their parent atoms; the temperature factors U_{iso} of hydrogen atoms were set as 1.2 times the U_{eq} value of the appropriate carrier atom.

Crystallographic data for the structural analysis has been deposited with the Cambridge Crystallographic Data Centre, No. 1029550 for the CoL. Copy of this information may be obtained free of charge from: The Director, CCDC, 12 Union Road, Cambridge, CB2 1EZ, UK. Fax: +44(1223)336-033, e-mail: deposit@ccdc.cam.ac.uk, or www.ccdc.cam.ac.uk.

Structure of the complex with atom numbering scheme is shown in Fig. 2 and selected bond lengths and angles are listed in Supporting Information file, Table S_2 Section (II). The cobalt atom is placed in a *trans*-CoN_4Cl_2 donor environment with four nitrogen atoms provided by the Schiff base ligand and two chloride atoms from the initial metal salt.The N_4-donor pocket of the Schiff base forms the basal plane and two chloride anions are located in the axial positions. The hydrazone ligand (HL) after deprotonation forms one six and two five-membered chelate rings. The Co–N and Co–Cl distances are in normal ranges observed in other reported cobalt complexes with the hydrazone ligand. The C2–O1, C2–N4 and C2–N5 bond lengths are 1.220 (3), 1.386(3) and 1.390(3) Å, respectively, which are close to the reported hydrazone based ligands that coordinate to the metal core in keto form, indicating that noketo-enol tautomerism happens on complexation. Moreover, these bond lengths are comparable to the C=O and C–N bond lengths in free cabohydrazone based ligands.[32] All of these finding demonstrate the elimination of amidic hydrogen without enolization through N5−C2−O1, which is confirmed by IR spectrum.[35] Structure of the crystal is stabilized by two intermolecular N4–H4···O2

and O2–H2···O1 hydrogen bonds, formed between methanol and complex molecules and creating a pseudo-dimer structure (Fig. 3).

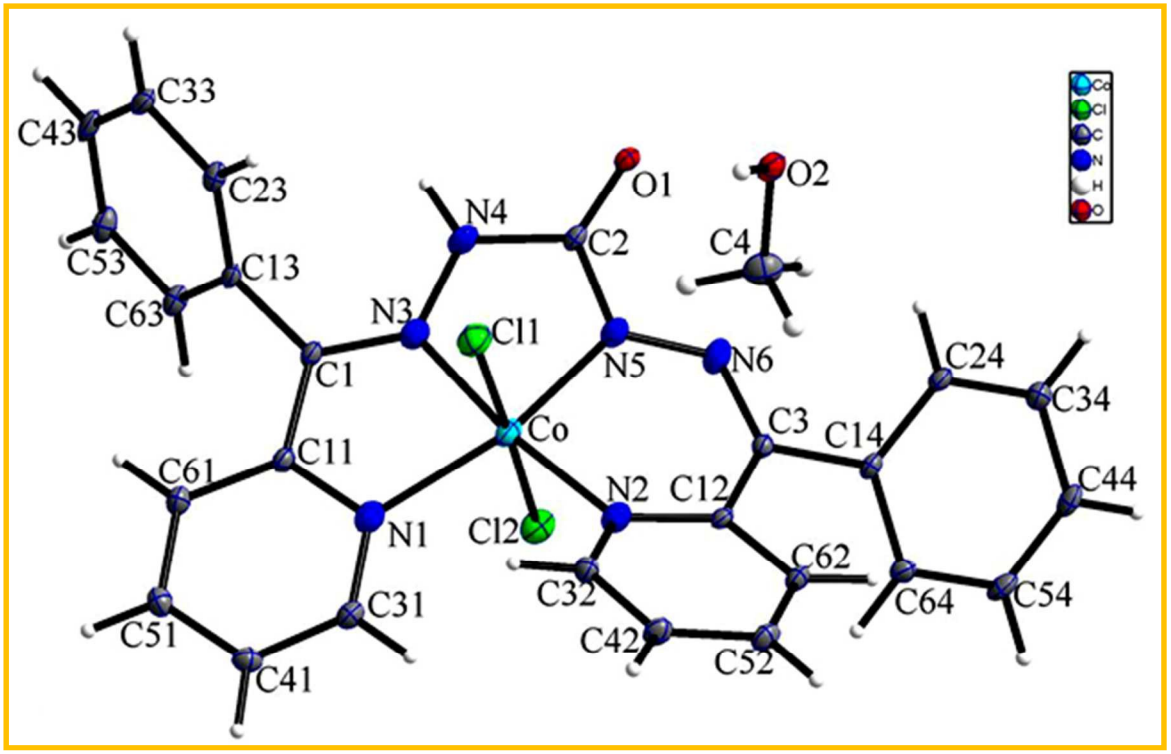

Fig. 2. Structure of complex CoL

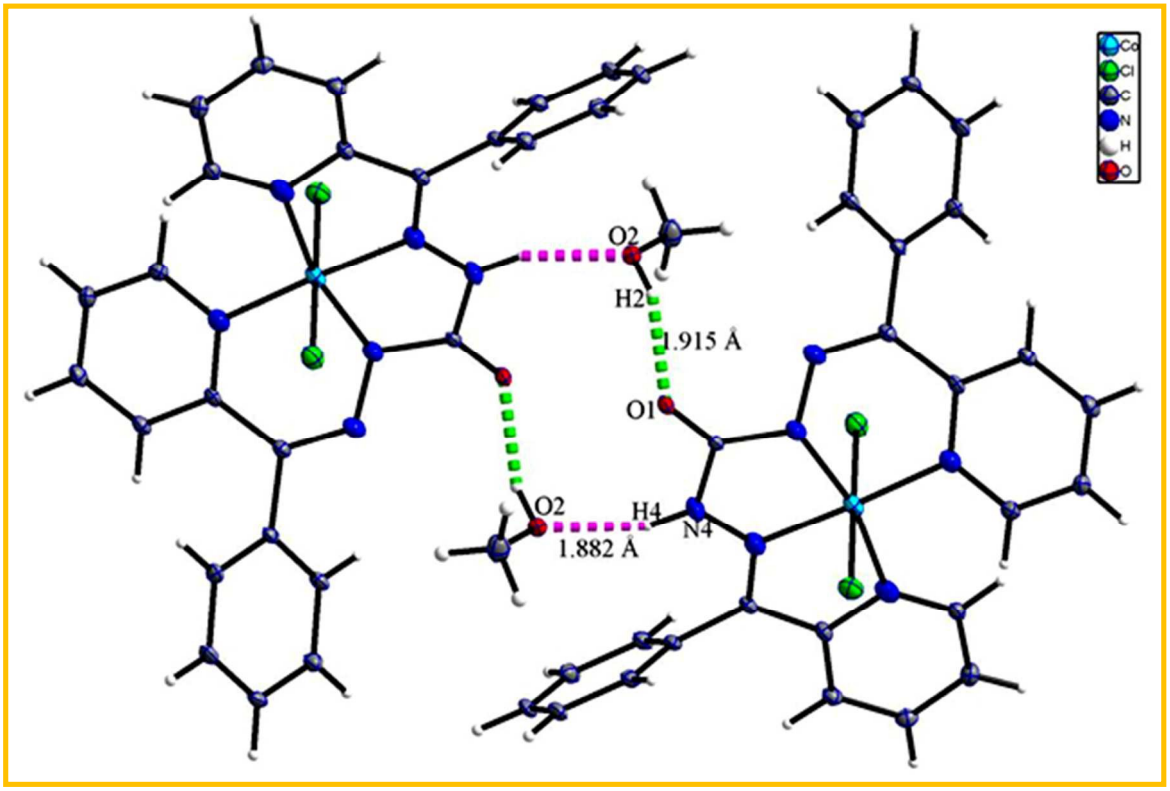

Fig. 3. Intermolecular hydrogen bonding in the crystal of CoL

To better understand the different forms of the CoL, additional UV−Vis measurements were performed using a 60 μM aqueous solution of the Co(III)-complex. As Fig. 4a is illustrated the CoL shows three peaks at 270, 390 and 510 nm. Drop wise addition of HCl to the solution resulted in a decrease of the absorption band at 510 nm (Fig. 4b). This indicates that a proton binds to the complex and changes its form, making it lipophilic.

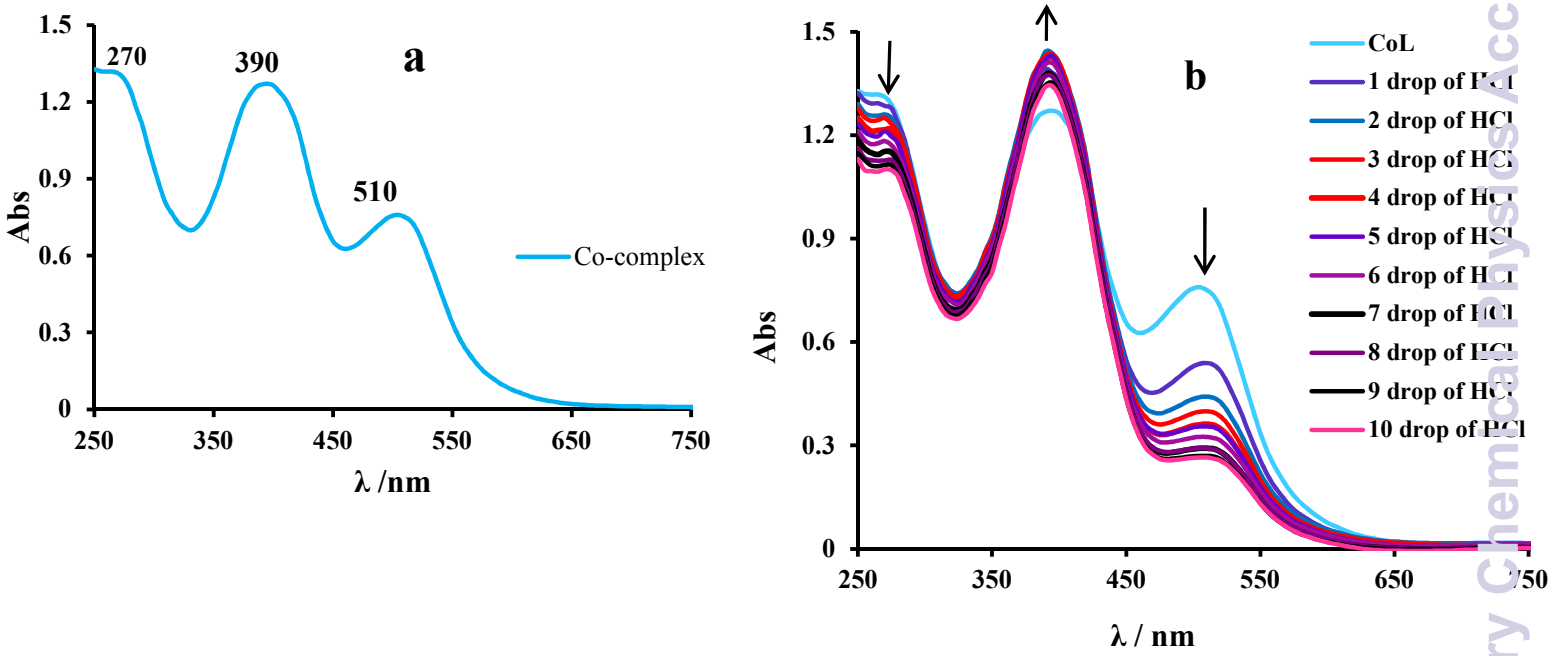

Fig. 4. (a) UV/Vis spectra of the CoL 60 μM in aqueous solution, (b) the effect of proton additions on the absorption peaks of the CoL

3.2. *Electrochemical biphasic studies of oxygen reduction catalyzed by the complex*

Fig. 5 compares the first scan of three cyclic voltammograms obtained by polarizing the water-DCE interface from -0.26 to 0.38 V. The potential region the interface behaves as a polarizable electrode is called the potential window. The supporting electrolytes, LiCl and BATB determine the size of the

potential window. When the aqueous phase is made very positive compared to the organic phase, either a cation in the aqueous phase transfers into the organic phase, or an anion transfers from the organic phase to the aqueous phase. The process taking place depends on the standard potentials of ion transfer. BA^+ and TB^- are very lipophilic ions or their transfer potentials are higher; therefore the transfer of Cl^- at negative potentials and H^+ at positive potentials limited the potential window. Compared to the background voltammetric response, only a small voltammetric with a half-wave potential at 0.0 V was observed after adding Fc to the organic phase. This voltammogram corresponds to the transfer of ferrocenium produced by a slow oxidation of Fc in the air-saturated stock solutions (Fig. 5). [14] When both the catalyst CoL and Fc were present, Fc^+ was produced at the interface and enhanced current with a half-wave potential at 0.0 V compared to the present only Fc in the organic phase. The voltammmetric signal at positive potentials corresponds to the proton coupled electron transfer reaction. These data suggest that the transfer of protons facilitated by the complex induces an oxygen reduction by Fc, thereby forming Fc^+.

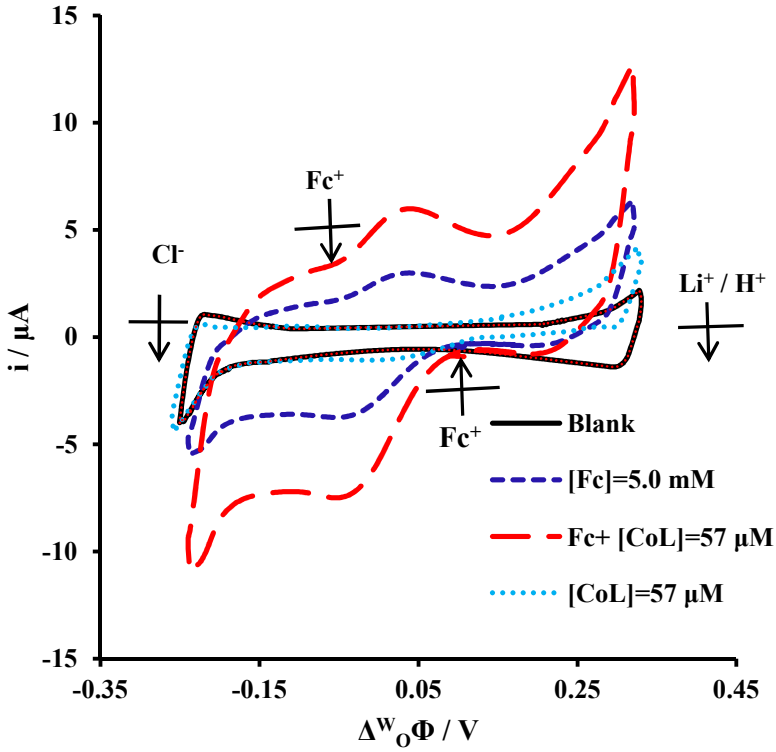

Fig. 5. CVs obtained at a water/1,2-DCE interface with the cell illustrated in Scheme 2: x = 0 and y =0 (solid line), x = 0 and y = 5 (black dotted line),x = 57 and y = 0 (blue dashed line), and x = 57 and y= 5 (red dashed line), Scan rate used: 50 mVs^{-1}.

Fig. 6 indicates the effect of pH on the PCET peak current increase and Fc^{+} ion transfer waves. As is seen the observed current shifts with pH by about 60 mV/pH, which is in accordance with the Nernst equations for the interfacial PCET reaction. [6, 15] Also, ion transfer waves of Fc^{+} were enhanced with decreasing pH, which shows that more Fc^{+} is generated with rising proton concentration, (see the mechanism of the proton pump, Scheme 4).

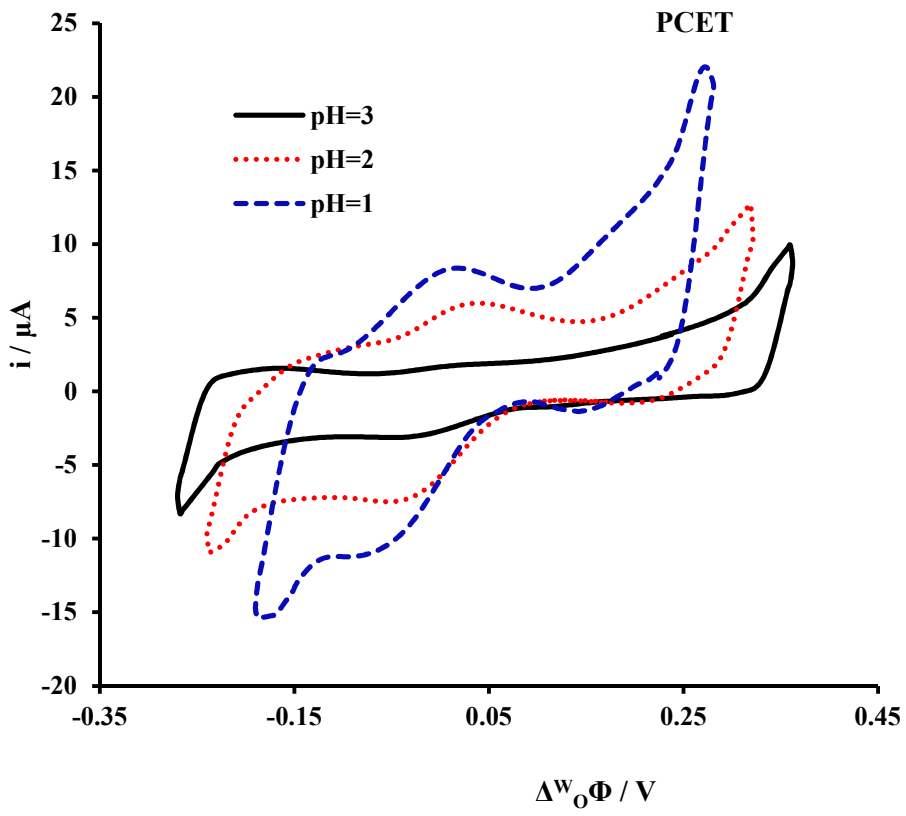

Fig. 6. Cyclic voltammetry at a water/1,2-DCE interface with the cell illustrated in Scheme 2, in the presence of 5 mM of Fc and 57 µM of CoL (x =57 and y = 5) at different pH, Scan rate used: 50 mVs^{-1}.

The observed PCET current and Fc^{+} formation also increase with increasing concentrations of the catalyst CoL in the range of 0-129 µM as shown in Fig. 7. The irreversible current depends on the oxygen concentration and is also directly proportional to the CoL concentration in the range of 0-129 µM, when O_2, Fc, and protons are in excess.

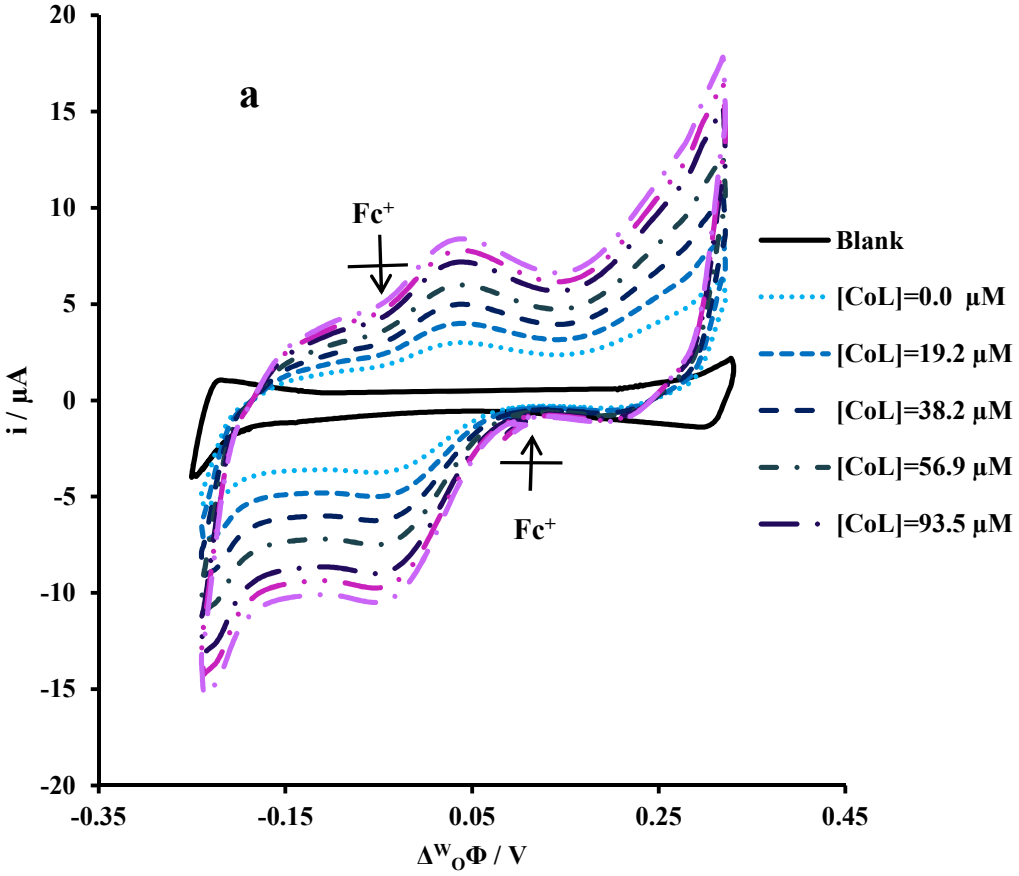

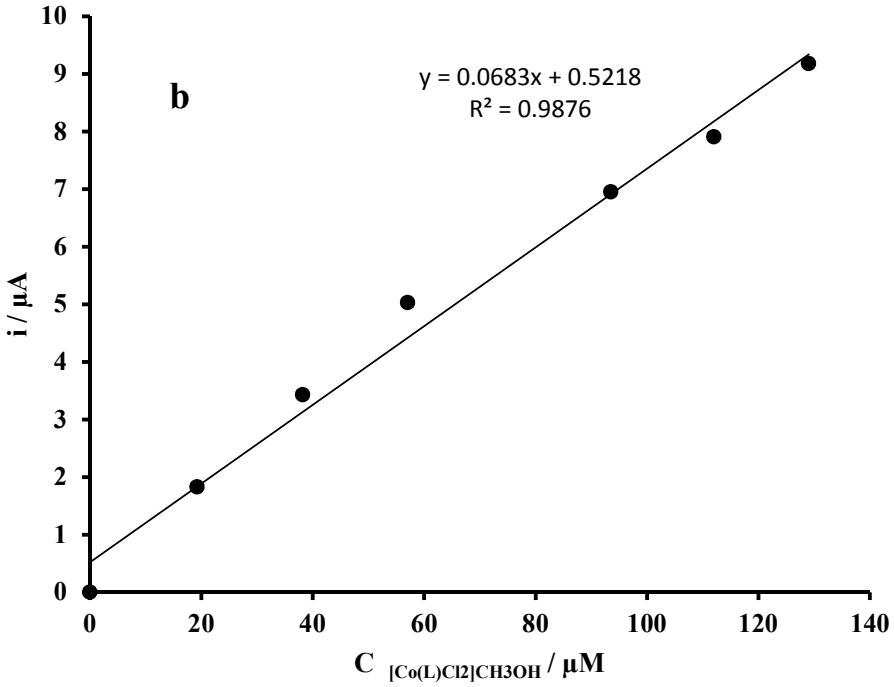

Fig. 7. (a) Cyclic voltammetry at a water-DCE interface obtained with the cell illustrated in Scheme 2 in the presence of 5mM Fc (y =5) and various concentrations of complex CoL, Scan rate used: 50 mVs^{-1}. (b) Linear dependence of the irreversible current at 0.35 V on complex CoL concentration

3.3. Two-phase shake flask experiments

Oxygen reduction can be explained by the Scheme 5, where the oxygen, CoL takes protons from the aqueous phase and electrons from the donor in the organic phase in a PCET step. The formed hydrogen peroxide is extracted into the aqueous phase.

Two-phase reactions controlled chemically by the distribution of ions, so-called shake-flask experiments. Typically, an aqueous solution containing the lithium tetrakis(pentafluoro phenyl)borate anion, LiTB (5 mM), and HCl (32 mM) was placed in contact with a DCE solution containing Fc (5 mM) and the CoL (57 μM). When TB^- is used as a common ion (dissolving 5m M of LiTB in water and 5mM of BATB in DCE). The two-phase reaction was carried out by stirring the reaction flasks for 50 min, after which the two phases were separated and the organic phase analyzed directly by UV-Vis, (Fig. 8), whereas the aqueous phase were titrated with KI. In the top aqueous phase in all three flasks of Fig. 8, (in the a, b and c parts), 32 mM HCl was present, while the DCE phase contained 57 μM CoL in flask 1, 5 mM Fc in flask 3 and both reagents in flask 5. The Galvani potential difference across the interface was calculated and found to be 0.536V, (Table 1, and Supporting Information, Section III).

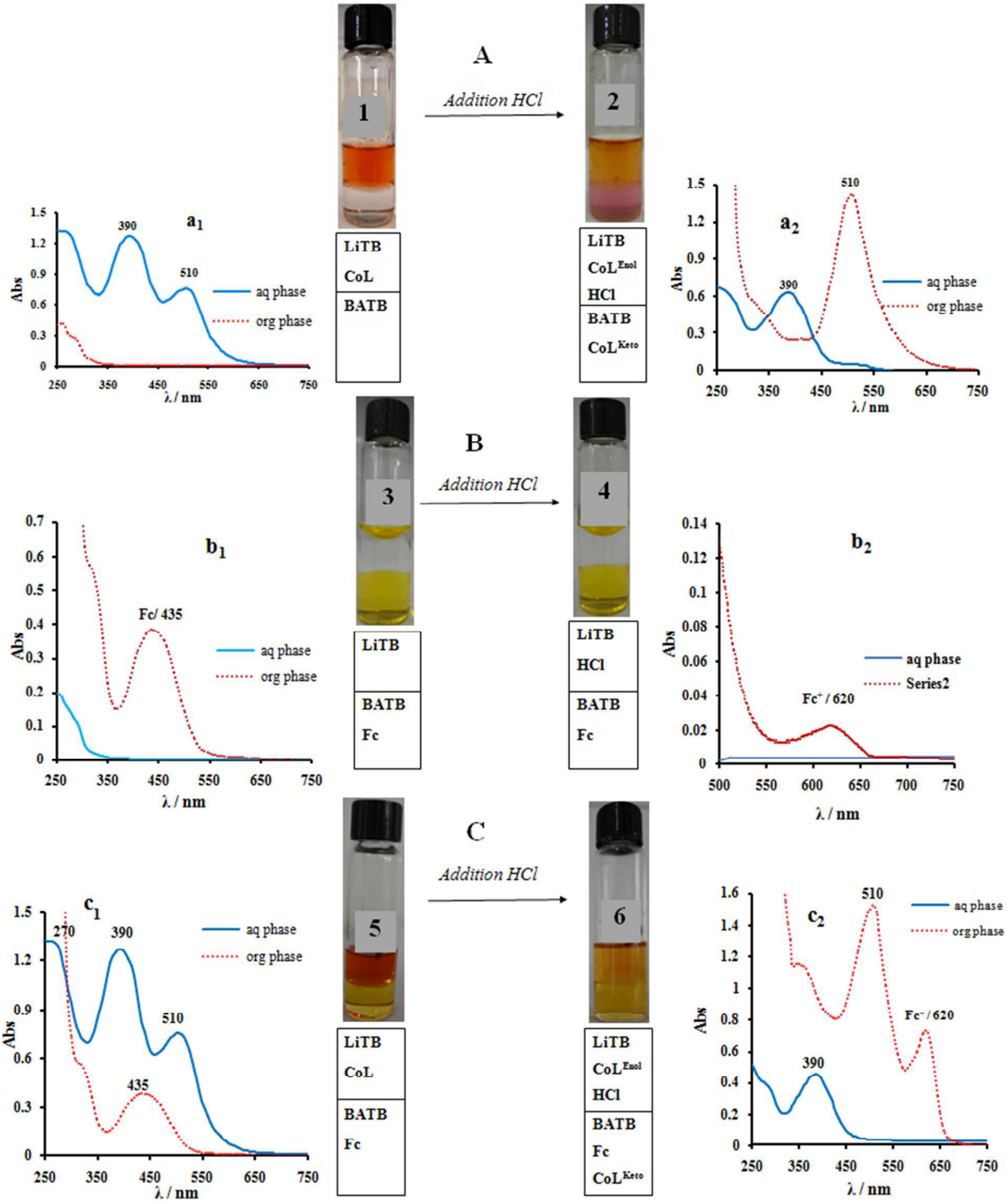

Fig. 8.(a) Photographs of two-phase reactions controlled by TB^- partition (shaking a 50 min): the top aqueous phase containing 5 mM LiTB + 57 μM CoL (flask 1) and 5 mM LiTB + 57 μM CoL + 32 mM HCl (flask 2) the bottom DCE phase contained 5 mM BATB was the same for two flasks and addition UV-visible spectra of the DCE (red line) and aqueous phase (blue line) before (a_1) and after (a_2) shaking and separated from each other are illustrated in Fig. 8a. (b) Photographs of two-phase after shaking a 50 min: the top aqueous phase containing 5 mM LiTB (flask 3) and 5 mM LiTB + 32 mM HCl (flask 4), the bottom DCE phase contained 5 mM BATB + 5 mM Fc was the same for two flasks, UV-visible spectra of the DCE (red line) and aqueous phase (blue line) before (b_1) and after (b_2) shaking and separated from each other are illustrated in Fig. 8b, (c) Photographs of two-phase (shaking a 50 min): the top aqueous phase containing 5 mM LiTB +57 μM CoL (flask 5) and 5 mM LiTB + 32mM HCl + 57 μM CoL (flask 6) the bottom DCE phase containing 5 mM BATB + 5 mM Fc was the same for two flasks, UV-visible spectra of the DCE (red line) and aqueous phase (blue line) before (c_1) and after (c_2) shaking and separated from each other are illustrated in Fig. 8c

Table 1. Calculated Equilibrium Concentrations after Contact with 5 mM BATB in DCE with 32 mM HCl and 5 mM LiTB in Water

	c_{H^+} /mM	c_{BA^+} /mM	c_{Li^+} /mM	c_{TB^-} /mM	c_{Cl^-} /mM
Water	27.023	6.490×10^{-21}	5.000	0.011	32.000
DCE	4.977	5.000	6.011×10^{-74}	9.988	3.089×10^{-17}

The Galvanic potential difference across the water/DCE interface calculated is approximately 0.536 V.

In fact, both the organic and aqueous phases in Fig. 8a, (flask 1), before addition of the catalyst CoL to aqueous phase are colorless. After the addition of the catalyst and HCl to aqueous phase then stirring for 30 min, the DCE phase changed from colorless to pink, which is indicative of the transmission of the catalyst from the aqueous phase to organic phase. The color of the aqueous phase

after addition of the catalyst was red, but after the transmission of the catalyst to the organic phase, changed to yellow. According to Scheme 1, the ligand (HL) has two tautomeric forms that cause the catalyst to show keto or enol structures in the aqueous solution. The keto and enol forms of the complex have a tendency to the organic and water phases, respectively (Fig. 8a). This tendency causes catalyst to be distributed between two phases. In order to support this postulate, the two phases were separated and air-dried. FT-IR spectra were obtained from the remaining solid catalyst in each phase FT-IR of the aqueous phase shows peaks at 3419 ,and 1630 cm^{-1} that can be attributed to the OH group of enol and C=N. The FT-IR spectrum of the organic phase shows peaks at 3100 and 1743 cm^{-1}, that can be attributed to the N-H and C=O stretching vibration. The aqueous phase does not show these peaks. Based on these observations we suggest the mechanism shown in Scheme 3 for the conversion of keto to enol form.

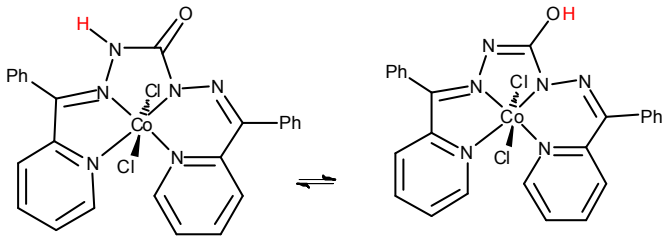

Scheme 3. Keto-enolinterconversion in the presence of H_3O^+

In the case when only Fc was present, (Fig. 8b, flask 4), it took much times to detect Fc^+ as the direct oxidation of ferrocene by oxygen is a very slow process. [15] In contrast, in the presence of both Fc and the catalyst CoL, (Fig. 8, flask 6), the color of DCE solution changed upon contact with the aqueous solution and the final color indicates a mixture of Fc^+ and the catalyst in the keto form. In the UV-visible spectrum (Fig. 8c, flask 6), an absorption band at 620 nm due to Fc^+ was observed. The conversion represents the ratio of Fc^+ (or catalysis activity) detected by UV/Vis spectroscopy (after 50 min of shake-flask reaction, before dilution) to the initial concentration of Fc was calculated 40% for Fc and the catalyst, but 1.2% for only Fc. Fig. 9 shows a time profile of the absorbance at 620 nm in the absence and presence of complex the catalyst. This figure illustrates much faster production of Fc^+ in the presence of complex the catalyst, suggesting the catalytic role of the complex in the reduction of O_2 by Fc.

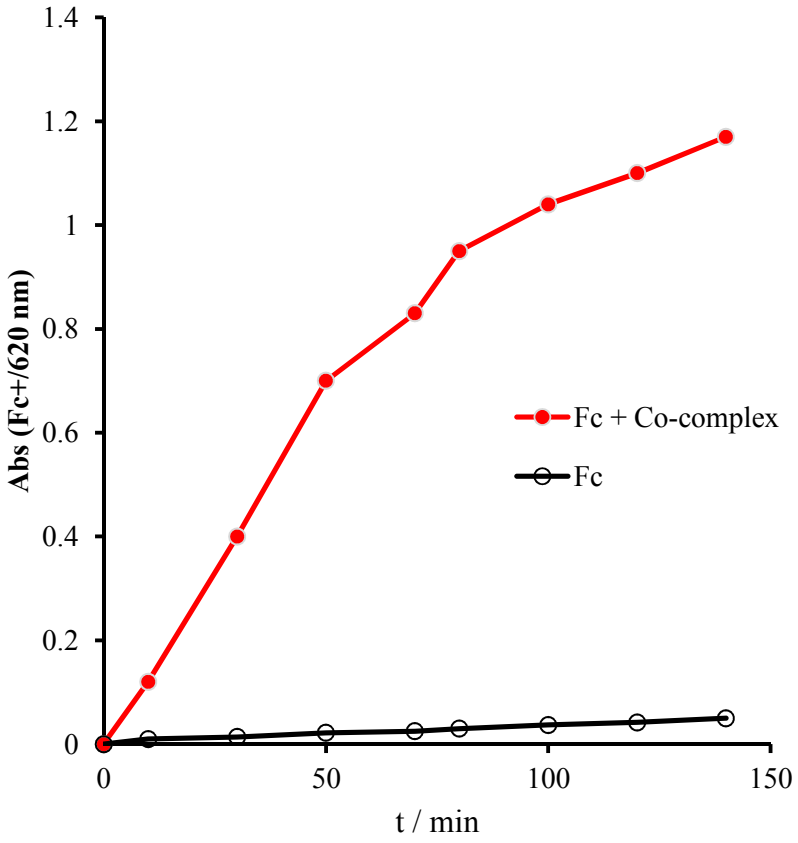

Fig. 9. Time evolution of the absorbance at 620 nm for the two-phase reaction in the absence ( ) and presence ( ) of 57 μM CoL

In order to determine the products of ORR, the aqueous solution were treated by excess KI and their UV-Visible spectra were measured (Fig. 10).One possible way to drive aqueous protons to the organic phase is by the addition of a very lipophilic anion to the aqueous phase. Here, we have used tetrakis(pentafluorophenyl) borate (TB^-) to form LiTB, and HTB in organic phase. After treating the aqueous phases with potassium iodide, (KI), hydrogen peroxide (H_2O_2) was detected only in the aqueous phase of Fig. 8c (flask6, CoL (57 μM) + Fc (5mM)). Hydrogen peroxide oxidizes iodide to triiodide, displaying two absorption bands at 285 and 350 nm as shown in Figure 10. All spectroscopic

data suggest that H_2O_2 is formed during the biphasic reaction in the presence of both Fc and CoL in DCE and aqueous phase respectively.

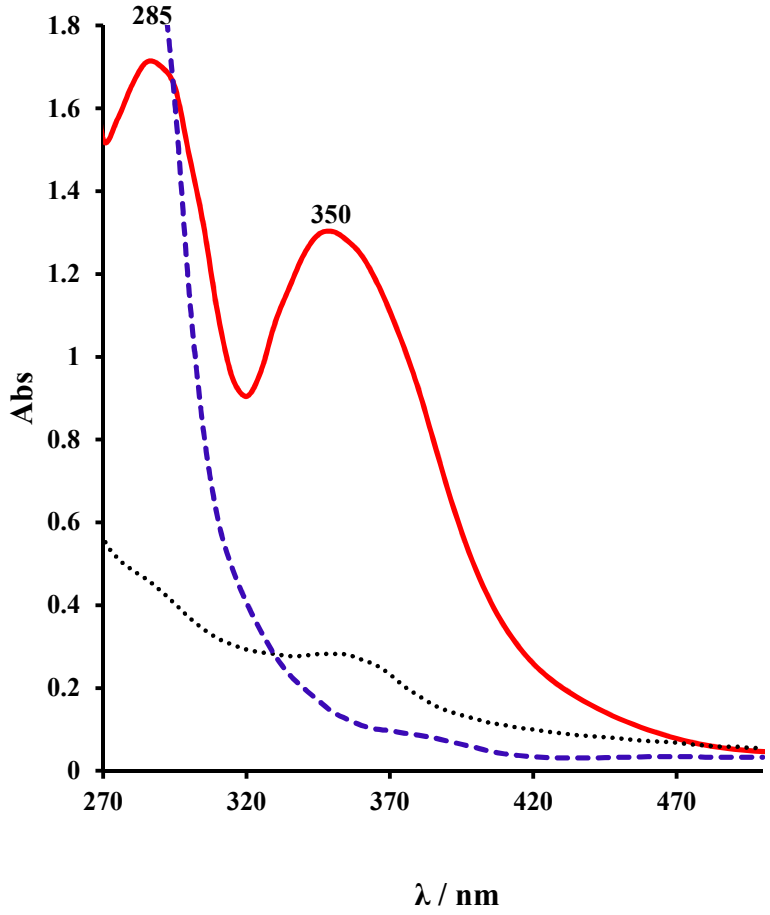

Fig. 10. UV-visible spectra of the aqueous phases separated from the flask 2 (dot line), flask 4 (dash line), and flask 6 (solid line) after being treated with excess KI for 20 min

The effect of hydrogen peroxide decomposition on the observed selectivity toward H_2O_2 was studied by using shake flask experimental that mixing equal volumes of DCE solution containing Fc and aqueous hydrogen peroxide and CoL solution in a vial (Scheme 4). The amount of hydrogen peroxide was determined with KI method decreased by 4% after 60 min. In this period of time, the most of the hydrogen peroxide was not decomposed, indicating that decomposition of H_2O_2 can be neglected over the total reaction time.

.

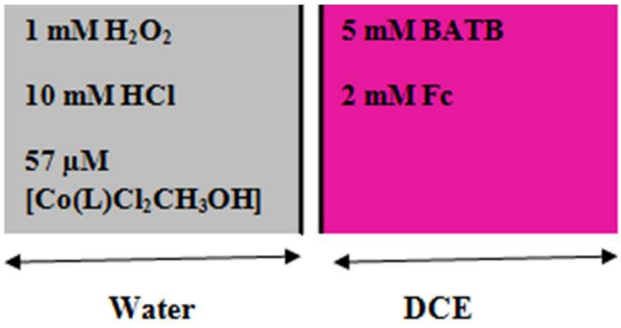

Scheme 4. Schematic representation of the initial composition of the aqueous phase and the organic phase for studying hydrogen peroxide decomposition in a biphasic reaction.

3.4. Gas phase proton affinity

Proton affinity (PA) is the gas phase basicity of donor atoms of a compound. PA values can help to understand many gas-phase reactions that are involved proton transfer. It is useful as a measure of correlation between acidity or basicity of organic compounds and their structure from the theoretical point of view.[36] The PA of a species A is the change of enthalpy of the following gaseous reaction in which 1 mol $H^+_{(g)}$ is consumed to form 1 mol of species $AH^+_{(g)}$.[37]

$$A + H^+ \longrightarrow AH^+ \quad (5)$$

$$PA = \Delta H_g^0(A^-) + \Delta H_g^0(H^+) - \Delta H_g^0(HA) \quad (6)$$

Gas-phase basicity is related to PA at constant temperature.[38] PA for four different proton acceptor sites of the most stable conformation of CoL, was calculated using B3LYP/6–31G** DFT method of *Spartan'08* program package, Scheme 5,[39] (Supporting Information, section IV).Calculations shown that the PAs are ranked as N1> N2 > O>N3 for all the donor sites. It means that N1 is the most basic position of CoL and the protonated form of N3 can be loose its proton more easily than the other.

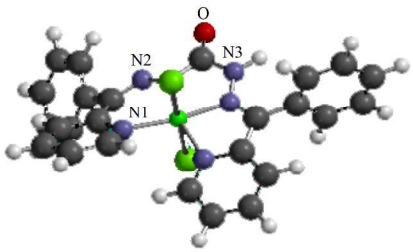

Ket

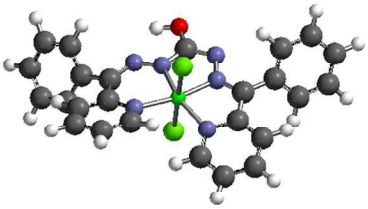

Enol

CoL

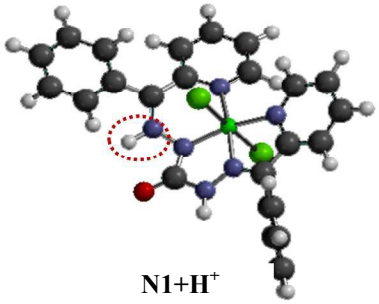

N1+H$^+$

(341.9), 0.16

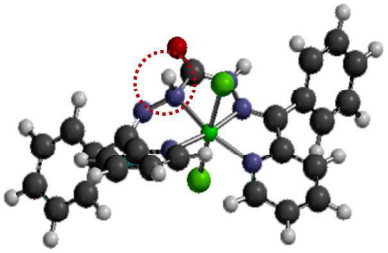

N2+H$^+$

(294.0), -0.63

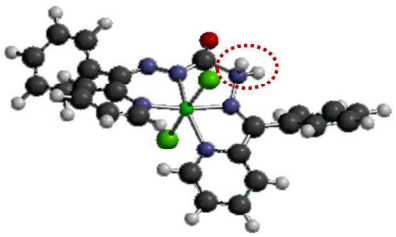

N3+H$^+$

(205.1), -0.63

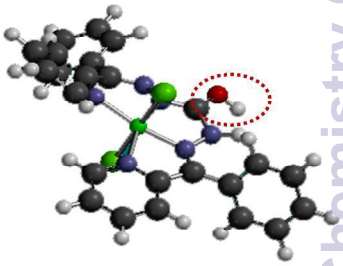

O+H$^+$

(287.3), 0.75

Scheme 5. The enol and keto forms of CoL, and the structure of all possible protonated forms of it. The PAs in kJ/mol and Log P are in parenthesis, respectively

Also, the Log P and molecular lipophilicity potential (MLP) of all species were calculated using the *MarvinView* program, Scheme 5 and Fig. 11.[40] As it seems, the keto form of CoL is more lipophilic than the enol form. This can be shifted the keto-enol equilibrium to produce more active keto form in the organic phase. Also, the aromatic rings of CoL form a relatively rigid and an extensive lipophilic region around the complex hydrophilic active site. This arrangement can be directed the substrate and increased the reaction rate. This conclusion can best be understood by comparison of the MLP of the both forms. Protonation of CoL can be increased its hydrophilicity, shifted the keto-enol equilibrium toward the keto form and transferred it into the aqueous phase. Among all four protonated forms of CoL,**O+H**$^+$ and tautomeric forms of **N3+H**$^+$ and **N2+H**$^+$ have more flatten active site with a similar hydrogen bond donor group (–OH), Scheme 5. All the results lead to the conclusion that the carbonyl group of the complex has a crucial role in the active site of the catalyst in both aqueous and organic phases.

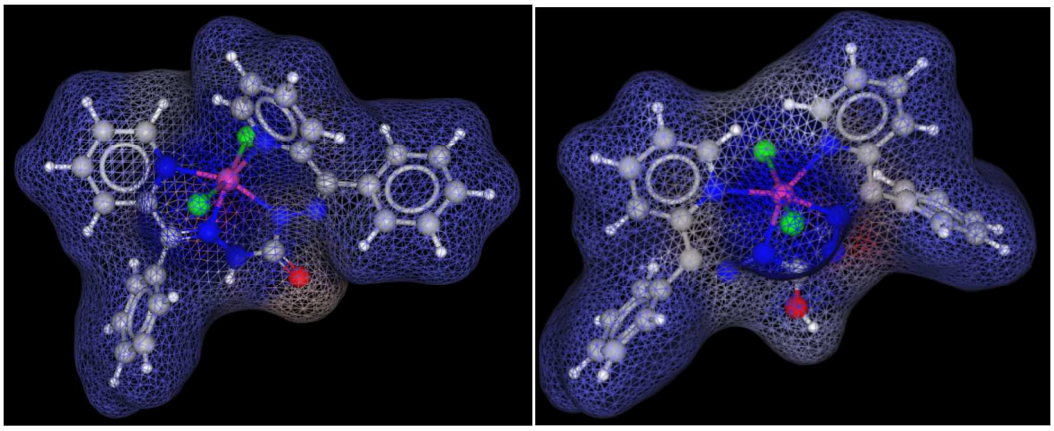

(a) (b)

Fig.11. The MLP of (a) the keto form (Log P = 3.88) and (b) the enol form (Log P = 3.73) of CoL. The red and blue colors show the most hydrophilic and the most hydrophobic regions, respectively

Based on the experimental results and the theoretical considerations, a four step reaction mechanism, similar to that proposed recently by Girault and co-workers,[9,14] is proposed as illustrated in Scheme 6. As, it was mentioned above, comparison of the MLP of the both forms of the catalyst CoL, showed that the keto form of CoL is more lipophilic than the enol form and moves to the organic phase,. Based on the mechanism, the proton transfer (PT) across the water/DCE interface and the electron transfer (ET) from Fc to the superoxide adduct, $[\{Co(+3)\text{-}L\}^{+}\text{-}O_2^{-}]$ are coupled at the phase boundary. This PCET reaction is preceded and followed by oxygen coordination to Co^{3+}-complex and the reduction of Co^{+3}-complex by Fc. These steps can be expressed by Equations 1-4.

$$[Co(+3)L]_{W}^{Enol} \rightarrow [Co(+3)L]_{DCE}^{Keto} \quad (1)$$

$$[Co(+3)L]_{DCE}^{+\,Keto} + Fc_{(DCE)} \rightarrow [Co(+2)L]_{DCE}^{Keto} + Fc_{(DCE)}^{+} \quad (2)$$

$$[Co(+2)L]_{DCE}^{Keto} + O_{2(DCE)} \rightarrow [Co(+3)L]_{DCE}^{Keto}\text{--}O_2^{-}]_{(DCE)} \quad (3)$$

$$[Co(+3)L]_{DCE}^{Keto}\text{--}O_2^{-}]_{(DCE)} + 2\,Fc_{(DCE)} + 2\,H^{+}_{(W)} \rightarrow [Co(+3)L]_{DCE}^{Keto} + 2\,Fc_{(DCE)}^{+} + H_2O_2 \quad (4)$$

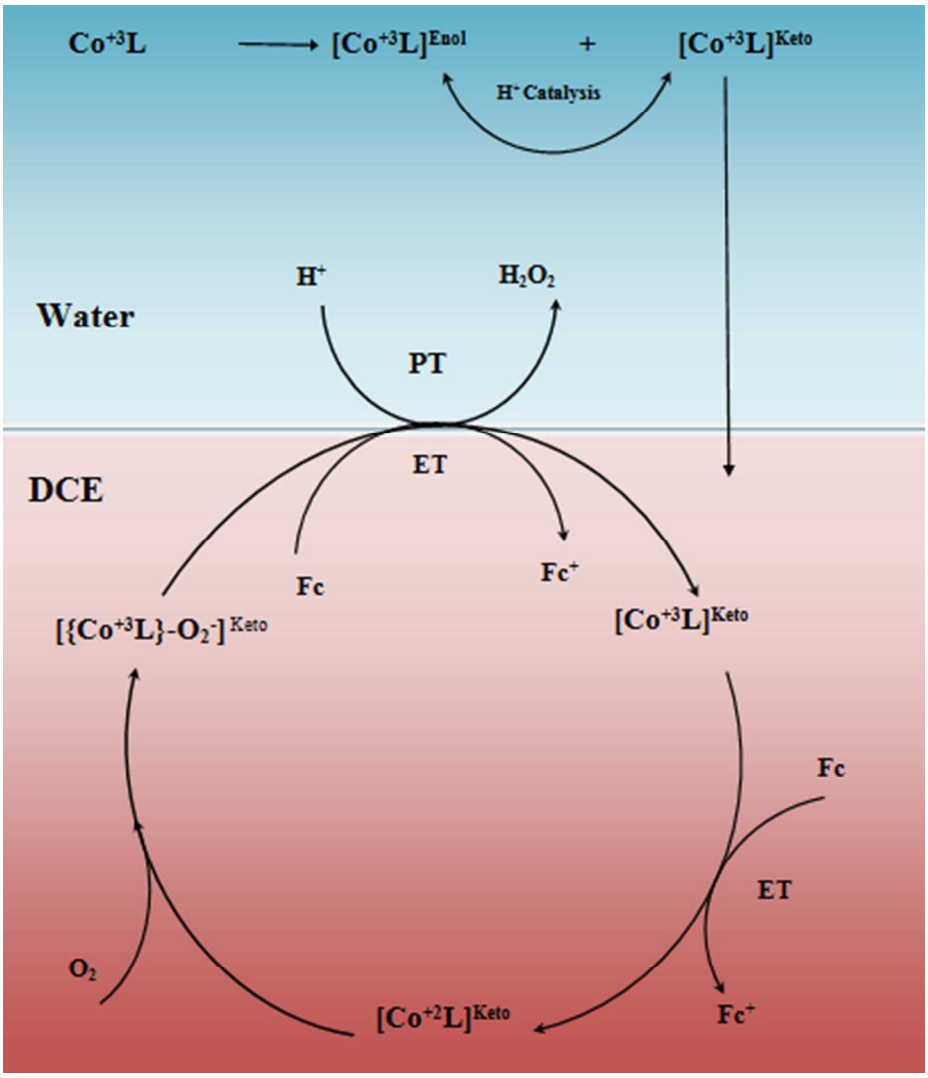

Scheme 6. Suggested mechanism for the proton pump controlled of the Galvani potential difference for O_2 reduction with Fc catalysed by CoL, PT= proton transfer, ET= electron transfer

4. Conclusions

In summary, a new complex of Co(III) with an oxidative stable carbohydrazone based ligand, (HL), was synthesized and characterized by elemental analyses and spectroscopic methods. The

compounds were fully characterized by X-ray diffraction analysis. The catalytic effect of the obtained complex on the proton-coupled oxygen reduction by Fc was studied at a water/DCE interface. Co served as a redox catalyst, activating O_2 for the reduction to H_2O_2. This study demonstrates the concept of interfacial molecular electrocatalysis for the reduction of oxygen, combining the use of molecular catalysts with electrochemical control.

The reaction can be started by driving protons to the oil phase by applying Galvani potential difference across the interface, which can be easily tuned by using common ion distribution or by the external potential polarization. The results show that Fc can be used as an electron donor for oxygen and hydrogen peroxide reduction, although the reaction without a catalyst is rather slow. This is mainly due to a very low electrochemical driving force. In the future this type of linked ferrocene could prove to be very interesting electron donors for oxygen reduction and hydrogen evolution, if the redox potential of the compound can be reduced, for example by methylation.

Acknowledgments

The authors are grateful to the University of Zanjan for financial support of this study.

References:

1 M.M. Walczak, C.A. Alves, B.D. Lamp and M.D. Porter, *J. Electroanal. Chem*., 1995, **396**, 103.

2 a) I. Yamanaka, T. Onizawa, S. Takenaka and K. Otsuka, *Angew.Chem. Int. Ed.,* 2003, **42**, 3653, b) V.R. Choudhary, A.G. Gaikwad and S.D. Sansare, *Angew. Chem. Int. Ed.*, 2010, **40**, 1776, c) I. Yamanaka and T. Murayama, *Angew. Chem*., 2008, **120**, 1926, d) K. Otsuka and I. Yamanaka, *Electrochim. Acta,* 1990, **135**, 319.

3 K. C. Lin, C. Y. Yin and S. M. Chen, *Sensor Actuat. B,* 2011, **157**, 202.

4 F. Yang, K. Cheng, X. Xue, J. Yin, G. Wang and D. Cao, *Electrochim. Acta,* 2013 ,**107**, 194.

5 F. Reymond, D. Fermin, H.J. Lee and H.H. Girault, *Electrochim. Acta.,* 2000, **45**, 2647.

6 M.A. Mendez, R. Partovi-Nia, I. Hatay, B. Su, P.Y. Ge, A.N. Olaya, M. Younan, M. Hojeij and H.H. Girault, *Phys. Chem. Chem. Phys*., 2010, **12**, 15163.

7 I. Hatay, B. Su, F. Li, R. Partovi-Nia, H. Vrubel, X. Hu, M. Ersoz and H.H. Girault, *Angew. Chem.,* 2009, **121**, 5241.

8 M.A. Me´ndez, R. Partovi-Nia, I. Hatay, B. Su, P-Y. Ge, A. Olaya, N. Younan, M. Hojeij and H.H. Girault, *Phys. Chem. Chem. Phys.,* 2010, **12**, 15163.

9 I. Hatay, B. Su, F. Li, M.A. Mendez, T. Khoury, C.P. Gros, J.M. Barbe, M. Ersoz, Z. Samec and H.H. Girault, *J. Am. Chem. Soc.,* 2009, **131**, 13453.

10 A. Trojanek, J. Langmaier and Z. Samec, *Electrochem. Commun.,* 2006, **8**, 475.

11 M. Suzuki, M. Matsui and S. Kihara, *J. Electroanal. Chem.,* 1997, **438**, 147.

12 H. Ohde, K. Maeda, Y. Yoshida and S. Kihara, *J. Electroanal. Chem.,* 2000, **483**, 108.

13 P. Liljeroth, B.M. Quinn and K. Kontturi, *Langmuir,* 2003, **19**, 5121.

14 B. Su, I. Hatay, A. Trojanek, Z. Samec, T. Khoury, C.P. Gros, J.M. Barbe, A. Daina, P.A. Carrupt, and H.H. Girault, *J. Am. Chem. Soc.,* 2010, **132**, 2655.

15 I. Hatay, B. Su, M.A. Mendez, C.M. Corminboeuf, T. Khoury, C.P. Gros, M. Bourdillon, M. Meyer, J.M. Barbe, M. Ersoz, S. Zalis, Z. Samec and H.H. Girault, *J. Am. Chem. Soc.,* 2010, **132**, 13733.

16 Y. Li, S.Z. Wu and B. Su, *Chem. Eur. J.,* 2012, **18**, 7372.

17 I. Hatay Patir, *Electrochim. Acta,* 2013, **87**, 788.

18 I. HatayPatir, *Electroanal. Chem.,* 2012, **685**, 28.

19 B. Su, I. Hatay, F. Li, R. Partovi-Nia, M. Méndez, Z. Samec, M. Ersoz and H.H. Girault, *Electroanal. Chem.,* 2010, **639**, 102.

20 PAC, Glossary of class names of organic compounds and reactivity intermediates based on structure (IUPAC Recommendations) 1995.

21 W. Plass, *Coord. Chem. Rev.,* 2003, **237**, 205.

22 M.R. Maurya, S.Khurana, C. Schulzke and D. Rehder, *Eur. J. Inorg. Chem.,* 2001, **2001**, 779.

23 a) R. Bikas, H. Hosseini-Monfared, T. Lis and M. Siczek, *Inorg. Chem. Commun*. 2012, **15** 151, b) H. Hosseini Monfared, R. Bikas and P. Mayer, *Inorg. Chim. Acta,* 2010, **363**, 2574.

24 a) P. Krishnamoorthy, P. Sathyadevi, P.T. Muthiah and N. Dharmaraj, *RSC Adv.,* 2012, **2**, 12190, b) M. Alagesan, N.S.P. Bhuvanesh and N. Dharmaraj, *Dalton. Trans.,* 2013, **42**, 7210.

25 P.A. Vigato and S. Tamburinii, *Coord. Chem. Rev.,* 2004, **248**, 1717.

26 J.P. Collman, L. Zeng and J.I. Brauman, *Inorg. Chem.,* 2004, **43**, 2672.

27 J.R. Carey, S.K. Ma, T.D. Pfister, D.K. Garner, H.K. Kim, J.A. Abramite, Z. Wang, Z. Guo and Y.A. Lu, *J. Am. Chem. Soc.,* 2004, **126**, 10812.

28 J.L. Sessler, J.W. Sibert, V. Lynch, J.T. Markert and C.L. Wooten, *Inorg. Chem.,* 1993, **32**, 621.

29 T. Aono, H. Wada, Y. Aratake, N. Matsumoto, H. Okawa and Y. Matsuda, *J. Chem. Soc., Dalton Trans.,* 1996, 25.

30 A. Pui, C. Policar and J-P. Mahy, *Inorg. Chim. Acta,* 2007, **360**, 2139.

31 K. Ambroziak, R. Pelech, E. Michert, T. Dziembowska and Z. Rozwadowski, *J. Mol. Catal. A: Chem.,* 2004, **211**, 9.

32 R. Bikas, P. Mahboubi Anarjan, S.W. Ng and E.R.T. Tiekink, *Acta Cryst. E.,* 2012, **68**, O193.

33 G.M. Sheldrick, *Acta. Cryst. A.,* 2008, **64**, 112.

34 V.J. Cunnane, D.J. Schiffrin, C. Beltran, G. Geblewicz and T. Solomon, *J. Electroanal. Chem. Interfacial. Electrochem.,* 1988, **247**, 203.

35 a) H. Hosseini-Monfared, R. Bikas, P. Mahboubi-Anarjan, A.J. Blake,V. Lippolis, N.B. Arslan and C. Kazak, *Polyhedron,* 2014, **69**, 90, (b) H. Hosseini-Monfared, R. Bikas, J. Sanchiz, T. Lis, M. Siczek, J. Tucek, R. Zboril, P. Mayer, *Polyhedron,* 2013, **16**, 45, (c) R. Bikas, H. Hosseini-Monfared and L. Sieroń, A. Gutiérrezc, *J. Coord. Chem.,* 2013, **66**, 4023.

36 W. Danikiewicz, *In. J. Mass Spectrum,* 2009, **285**, 86.

37 S. Hwang, Y-H. Jang and D-S. Chung, *Bull. Korean Chem. Soc.,* 2005, **26**, 585.

38 Z. Ying. Y. Jiang, X. Du, G. Xie, J. Yu and H. Wang, *Sensor. Actuat. B.,* 2007, **125**, 167.

39 ***Spartan'08,*** Wavefunction, Inc., Irvine, CA.

40 Calculator Plugins were used for structure property prediction and calculation, MARVIN 6.3.0, 2014, ChemAxon, http://www.chemaxon.com